Exp Fluids
DOI 10.1007/s00348-008-0573-6

RESEARCH ARTICLE

Flow visualization using tobacco mosaic virus

David L. Hu · Thomas J. Goreau · John W. M. Bush

Received: 26 May 2005 / Revised: 15 September 2008 / Accepted: 17 September 2008

Abstract A flow visualization technique using dilute solutions of tobacco mosaic virus (TMV) is described. Rod-shaped TMV-particles align with shear, an effect that produces a luminous interference pattern when the TMV solution is viewed between crossed polarizers. Attractive features of this technique are that it is both transparent to the naked eye and benign to fish. We use it here to visualize the evolution and decay of the flows that they produce. We also report that dilute solutions of Kalliroscope are moderately birefringent and so may similarly be used for qualitative in situ flow visualizations.

1 Introduction

For many years, engineers have known that certain fluids and solids become temporarily birefringent or doubly refractive (able to refract light in two different directions) when subjected to shear. This effect is best observed when the birefringent material is placed between crossed polarizers; the transmission of light generates interference fringe patterns whose intensities are related to the magnitude of the strain rate of the material (Wayland 1960). Physically, such birefringence results from stretching, deformation or orientation of chiral polymer-like chains or suspended macromolecules (Pih 1980). The effect was used extensively in photoelastic stress analysis in solids, recently employed by the biolocomotion community to visualize the forces applied by crawling cockroaches (Full et al. 1995) and burrowing worms (Dorgan et al. 2005). Maxwell (1873) developed an analogous technique to visualize fluid motion, which became the subject of intense study in the 1950s. Here, we report on a plant-virus based birefringent technique that may ultimately prove useful to workers in biolocomotion and microfluidics.

Reviews of birefringence from the perspective of a chemist, fluid mechanician and engineer are given by Cerf and Scheraga (1952), Peterlin (1976) and Pih (1980), respectively, and are summarized here. Birefringence was first used to ascertain the shape of particles in colloidal suspensions (Diesselhorst and Freundlich 1916). Freundlich (1926) found that anisotropic particles such as rods or disks align with their long axis parallel to shear. A solution of such particles is birefringent if two conditions are satisfied: the particle's short axis is shorter than the wavelength of light and the particle's refractive index differs from that of the surrounding solution. Solutions of rods and disks become birefringent under different lighting conditions: specifically, for rods, the incident light must be normal to the flow direction; for disks, the incident light must be parallel to both the direction of flow and the disk face. Further investigations showed that many synthetic chemicals are birefringent, including colloidal suspensions of vanadium pentoxide (Humphrey 1922), milling dianthrapyrimidine

Electronic supplementary material The online version of this article (doi:10.1007/s00348-008-0573-6) contains supplementary material, which is available to authorized users.

D. L. Hu (✉)
Department of Mechanical Engineering,
Georgia Institute of Technology, Atlanta, GA, USA
e-mail: hu@me.gatech.edu; dhu@cmis.nyu.edu

T. J. Goreau
Global Coral Reef Alliance, 37 Pleasant Street,
Cambridge, MA 02139, USA

J. W. M. Bush
Department of Mathematics,
Massachusetts Institute of Technology,
Cambridge, MA 02139, USA

yellow solution (Prados and Peebles 1958) and aniline blue which provides rainbow-colored interference patterns (Freundlich 1926). While such man-made chemicals are generally harmful to animals, other naturally-arising compounds, such as tobacco mosaic virus (TMV), provide unexplored potential for organic flow visualization.

Current techniques that are safe for animals rely on following inert tracer particles, a technique known as digital particle image velocimetry (DPIV). Here, the fluid is seeded with micro-particles, and a plane within it is illuminated by a laser light sheet and tracked by computer in order to infer particle trajectories and fluid streamlines. This technique has been successful in visualizing the wakes behind fish (e.g. Drucker and Lauder 1999; Muller et al. 1997), copepods (Stamhuis 1995) and birds (Spedding et al. 2003). In addition to DPIV, there exist more convenient qualitative techniques that provide immediate results without computational analysis. Dyes such as fluorescein, ink and thymol blue (Merzkirch 1974) have been injected into the wakes of jellyfish (Dabiri et al. 2005), squid (Bartol et al. 2001) and insects (Hu et al. 2003). Such dye streamers generally are not well suited for fish, which are notoriously uncooperative. One alternative was proposed by Rosen (1959), who used a thin layer of milk to visualize fish wakes, from which some quantitative information was gleaned (Videler et al. 1999). Another alternative is the Schleiren technique in which a fish swims through a thermally stratified fluid, disrupting the stratification of refractive index, whose disturbances are shown by shadowgraphic projection (McCutchen 1977; Fiedler and Nottmeyere 1985). TMV provides an advantage over many of these techniques because, as we show in Sect. 2, it can be safely inhaled by fish and need not be seeded directly in their path.

The structure of the TMV molecule was deduced using birefringent techniques, revealing that it is a long cylinder with length 300 nm and diameter 18 nm (Takahashi and Rawlins 1933). Bawden et al. (1936) were the first to demonstrate its potential for safely visualizing the flow around animals: with photographers, Ramsey and Muspratt, they used TMV to illuminate the boundary layer around a swimming goldfish. Fritz Goro, Time-Life science photographer from 1937–1978, also photographed a fish using TMV and published his pictures in 1941 (reprinted here in Fig. 1). Neither investigators reported the details of their technique, which we reverse-engineer in Sect. 2. Sutera (1960) developed an apparatus to calibrate the TMV technique, and his results can be applied to study animal-generated flows.

While it is beyond the scope of this report to use TMV as a quantitative technique, we briefly describe here how it can be done (Appendix B, Sutera 1960). Consider a birefringent fluid sandwiched between two crossed polarizing filters called the polarizer and analyzer respectively

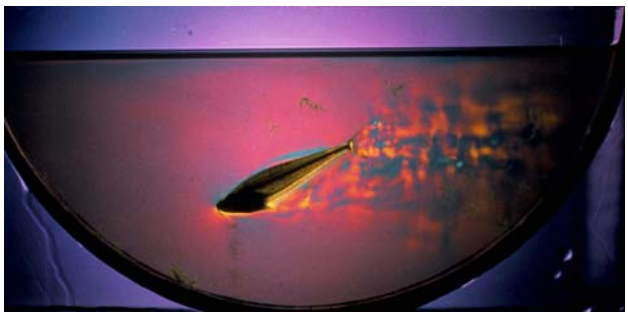

Fig. 1 The luminous wake of a fish swimming in a bowl of TMV solution, photographed by Fritz Goro (Goreau et al. 1993), whose methods were never published. Goro likely used three lights, *red*, *yellow* and *blue* to create the three wavelengths of light visible in the wake. The magnitude of the light intensity is related to the magnitude of the shear rate (Wayland 1960). The *purple* boundary layer adjoining the fish indicates a high degree of shear. Photo courtesy of T. Goreau

(Fig. 2). The light intensity I_1 at the recording plane may be expressed as

$$I_1 = \alpha I_0 \sin^2(\Delta\theta/2) \sin^2 2\phi \tag{1}$$

where I_0 is the incoming light intensity, α is the absorption coefficient through the light path and ϕ the angle between the plane of initial polarization and the principal vibration axis of the birefringent fluid. The optical phase difference of the light exiting the fluid, $\Delta\theta = 2\pi\frac{d}{\lambda}\Delta n$ where d is the length of the optical path in the medium, λ the wavelength of light and Δn the difference in indices of refraction of the birefringent solution (Pih 1980). Equation 1 shows that for a monochromatic light source, there are two conditions that extinguish light, causing I_1 to be zero. First, when $\Delta\theta/(2\pi)$ = 0,1, 2,..., dark fringes called isochromatics are produced. Second, when ϕ is 0 or $\pi/2$, dark fringe lines called isoclines are produced.

The amount of birefringence of the fluid, Δn, is given by orientation theory for rod-shaped particles (Wayland 1960):

$$\Delta n = \frac{4\pi}{15}\frac{G}{n}\frac{cEb}{D}\left[1 - \frac{E^2}{18D^2}\left(\sin^2 2\Lambda_0 + \frac{6b^2}{35}\right)\right], \tag{2}$$

where G is the optical anisotropy factor for the particles, n the mean index of refraction of the solution, c the volume concentration of the particles, $b = \frac{a_1^2 - a_2^2}{a_1^2 + a_2^2}$ the shape factor of the particles where a_1 is the rod length and a_2 its diameter, D the rotary diffusion constant for Brownian motion, E the magnitude of the principal strain rate and Λ_0 the angle between the principal strain rate axis and the streamline direction at the point of observation.

The position of the isoclines also gives information about the flow. Specifically, birefringence causes the isoclines to be phase shifted from the crossed axes of the polarizers by any angle χ

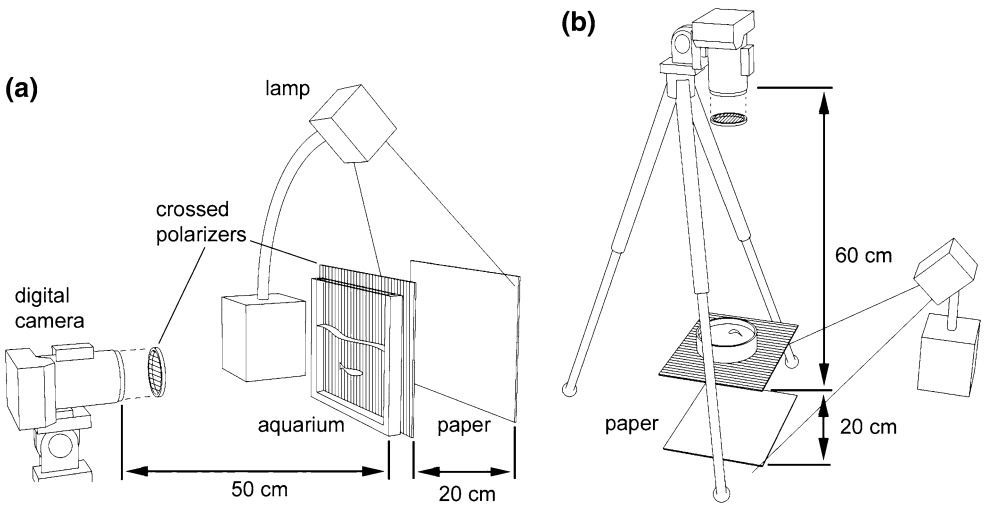

Fig. 2 The experimental apparatus. A dilute suspension of TMV is illuminated with polarized light, and viewed through a crossed polarizer. The arrangement for viewing (**a**) from the side, and (**b**) from above

$$\chi = -\frac{\gamma_s}{12D}\left[1 - \frac{1}{27D^2}\left(\frac{\gamma_s^2}{4} + \frac{24b^2}{35}E^2\right)\right] \quad (3)$$

where $\gamma_s = 2E \sin^2\Lambda_0$ is the shear rate parallel to the streamline. The theory (1)–(3) has been confirmed experimentally by Sutera (1960). In addition, a number of investigators have proposed theories allowing them to use birefringent data to gather quantitative information. Binnie (1945) used the birefringent solution benzopurpurin as a turbulence indicator in pipe flow: he finds that the greatest chromatic intensity appears at Reynolds numbers 1,970–2,900. Pindera and Krishnamurthy (1978) used lasers to determine the properties of a birefringent fluid. Prados and Peebles (1958) characterized the laminar flow around a cylinder, and Alcock and Sadron (1935) the flow between pairs of plates and between rotating cylinders. These studies show that birefringent fluids can be used in a quantitative manner. We now turn to a relatively new application of TMV, its use in visualizing animal-generated flows.

2 Experiments

We filled the apparatus in Fig. 2 with TMV solution to visualize the flows generated by black neon tetra fish (Figs. 3, 4, 5, 6, 7), jets (Fig. 8) and rising bubbles (Fig. 9) generated by a syringe. The apparatus was housed in a darkened room, with lighting provided by a 250 W tungsten–halogen lamp (Vision Research, Inc., North Star) reflected off a white sheet of paper. The birefringent fluid was sandwiched between two crossed linear polarizers (polarizing film, 40 by 30 cm by Edmund Industrial Optics; Techspec polarizing lens 58 and 37 mm by Crystal Vision). The color of the fluid, as observed by the polarizer farthest from the light source, was recorded by a digital video recorder (Sony, DCR-TRV950) and digital still

Fig. 3 A black neon tetra fish flaps its fins in a TMV solution. The luminous areas are indicative of the fluid shear generated by its fins and inhalation by its mouth. *Scale bar* 1 cm

camera (Sony, DSC-F707). We obtained side views using a glass tank (length 30 cm, span 1.5 cm, water depth 10 cm, Fig. 2a) and top views using a petri dish (diameter 14 cm, depth 2 cm, Fig. 2b) filled with the TMV solution (Fig. 2b).

Black neon tetra, common tropical fish, were obtained from our local pet store in New York and housed together in a filtered, oxygenated, heated aquarium under a 12 h light cycle. Fish housing and experiments were approved by the NYU committee on animal welfare (protocol number 07-1289). While the plant virus TMV has never been reported to infect animal hosts, we took precautions by immersing the fish in a low concentration of TMV (18 parts/million) for a short duration (min/trial). At the conclusion of the experiments, the fish appeared unaffected by the TMV solution and continued in good health until the end of their natural lives nearly a year later.

The preparation of TMV for use in flow visualization is described by Boedtker and Simmons (1958). Our TMV

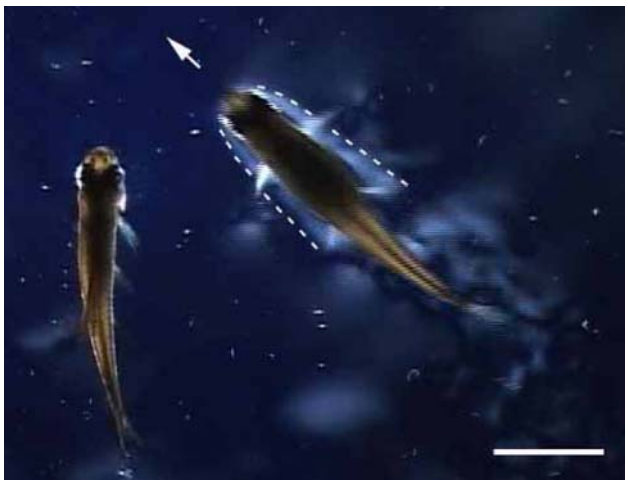

Fig. 4 The shear layer generated by a fish accelerating from rest. As the fish on the right accelerates in the direction of the *arrow*, it is adjoined by a luminescent boundary layer, marked by the *dotted lines*, indicative of the intense local shear. The fish on the *left* has a *dark outline*, consistent with its stationary state. *Scale bar* 1 cm

solution, obtained by juicing TMV-infected tobacco leaves, was donated by Deutsche Sammlung von Mikroorganismen und Zellkulturen (DSMZ). This solution was diluted to a concentration 0.4 ± 0.05 mg/mL using tap water and stored at 5°C. The solution was warmed to the fish's body temperature of 27°C before experiments. This particular dilution of TMV was optimal for flow visualization using our experimental apparatus: further dilutions provided insufficient contrast to visualize flow, while higher concentrations substantially increased the fluid viscosity and so altered the dynamics of the fish. TMV has been studied previously for its non-Newtonian properties (Wada 1954); the viscosity of TMV as a function of concentration has also been described in detail by Welsh (1955), who found that its viscosity decreases as the solution settles. To reduce the effects of settling, the TMV solution was shaken by hand and cleansed between experiments by passing the solution through filter paper. Following these procedures for our 0.4 ± 0.05 mg/m TMV solution, we measured a dynamic viscosity v of 1.89 cS.

We observed top and side views of the fish, visualizing the surrounding flows by observing the colors of the TMV solution. The fish had a characteristic length L of 3 cm and body speeds U of 2–5 body lengths/s. It generated flows characterized by a Reynolds numbers of $Re = UL/v = 950-1{,}500$ and a Strouhal number of $St = 2Af/U = 0.5-0.7$ where A is the tail-flap amplitude and f its frequency. In interpreting our observations, we note that TMV provides a cumulative picture of the flow, averaged over the depth of the fluid along the line of sight. Generally, white regions indicate both a higher shear rate and Reynolds number than dark blue regions (Sutera 1960; Binnie 1945). Our experiments with the fish indicate that in shear layers, the TMV solution changes color from black to bluish-grey at a Reynolds number of 250 and saturates at white at a Reynolds number of 1,600.

In Fig. 3, the fish "hovers" underwater by flapping its fins to transfer momentum downward, generating a luminous wake of vortices. In addition, inhalation by the fish

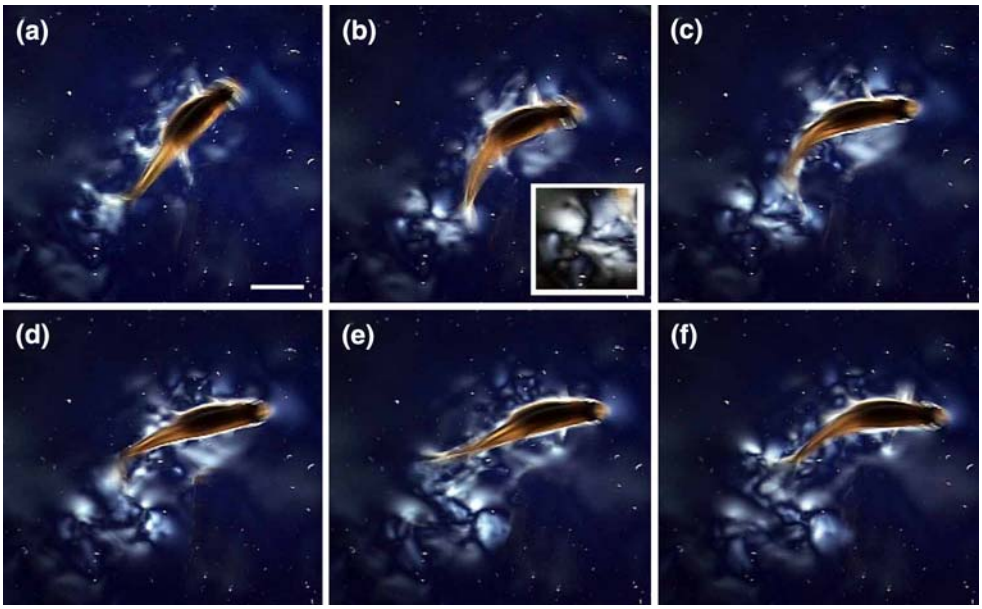

Fig. 5 The generation of a single vortex by a fish's tail. (**b–f**) The vortex appears as a coherent 1-cm diameter *white spot* crossed by *dark fringes*. These isoclines, a characteristic of birefringent techniques, result from the extinction of light by the crossed linear polarizers. Time between frames, 1/30 s. *Scale bar* 1 cm

Fig. 6 The reverse Karman vortex wake generated by a fish swimming from left to right. **a** *Side view*; **b** *top view*. The most recent vortices appear as coherent white spots; older vortices have slowed and decreased in their luminosity. *Scale bar* 1 cm

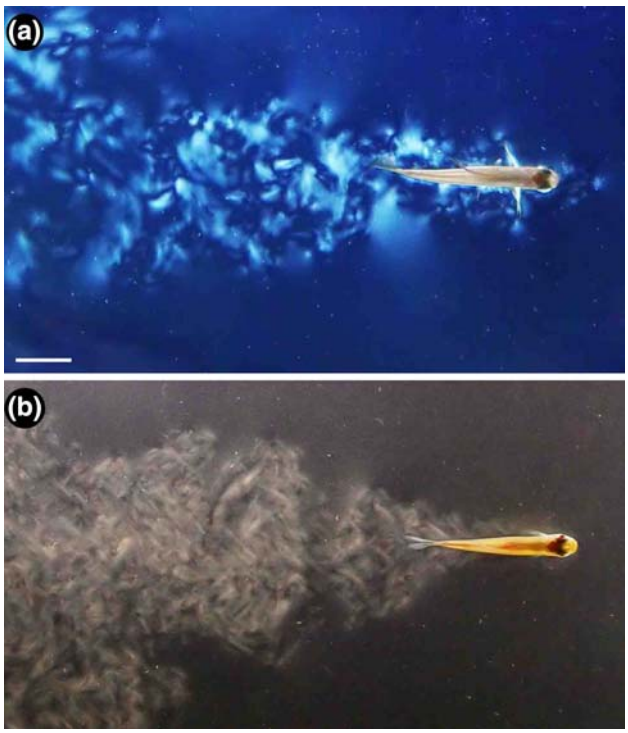

Fig. 7 Turbulent wakes generated by a fish decelerating in (**a**) TMV and (**b**) Kalliroscope solutions. (**a**) *Top view* in TMV shows a conical turbulent wake. To stop, the fish extends its pectoral fins and exhales a vortex ring. (**b**) In Kalliroscope solution between crossed polarizers, a turbulent wake is again evident. *Scale bar* 1 cm

generates a suction flow, which appears as a glowing white cone. When moving forward, the fish flaps its tail fin to propel itself using a carangiform mode of undulatory propulsion. As the fish accelerates from rest, it generates a luminous silhouette indicative of the high degree of shear in its boundary layer (Figs. 1, 4, 5, 6b). Since no light strip appears when the fish is static (Fig. 4) we infer that the light strip is not generated by refraction from the fish scales, but is instead indicative of a shear layer in the fluid.

To gain speed, the fish flaps its tail to generate a single vortex, visible as a coherent white spot (Fig. 5). Centered on the vortex are dark bands, isoclines marking the extinction of light by the crossed polarizers (Fig. 5b', Zocher 1921). A series of vortices appears as a reverse Karman vortex street, consisting of regions of high vorticity alternating in sign on either side of the fish's trajectory (Fig. 6, Videler et al. 2004). The supplementary video shows the generation of these vortices in real time. The fish's wake appears different at high speeds: it is triangular and turbulent, as shown in Fig. 7. We note that this wake structure is reminiscent of that created by a point source of momentum; here, the momentum is provided by the fish's driving strokes. To stop, the fish extends its pectoral fins and blows a vortex ring (Fig. 7a), a behavior first reported by McCutchen (1977). These figures demonstrate the versatility of qualitative TMV visualizations. While the sign or direction of the shear cannot be discerned without the technical methods applied by Sutera (1960), their relative magnitude can be discerned by the intensity of light observed.

We note that flows may also be visualized to some extent using a low dilution (10^{-4} mg/mL) of Kalliroscope that may be briefly tolerated by fish (Fig. 7b). Kalliroscope has a lower optical activity than TMV, as seen by the lower range of light intensity, making the vortex structure and boundary layers less apparent. We thus recommend TMV over Kalliroscope techniques.

We also visualized simple two-dimensional flows in a thin glass tank (length 30 cm, depth 10 cm, span 0.3 cm). In Fig. 8a, a syringe was used to produce suction, generating a radially symmetric region of high shear near the syringe tip. When a stream of TMV solution is forced back out of the syringe at low speeds (15 cm/s, Re = 80), we observe a coherent jet with the same diameter as the syringe (Fig. 8b). This jet appears white, reflecting its high shear rate relative to the quiescent background fluid. As the flow rate is increased to 30 cm/s (Re = 160), the jet grows turbulent (Fig. 8c) and generates regions of shear a few cm lateral to the main flow. TMV works equally well to reveal the stress fields generated by rising bubbles (Fig. 9a–c). TMV shows that bubbles of diameter 3 mm zig-zag as they rise, while smaller bubbles rise vertically (Fig. 9d).

3 Discussion

Before the digital age, the determination of flows and stress fields was accomplished with birefringent fluids and solids. These optical techniques have been all but been replaced by

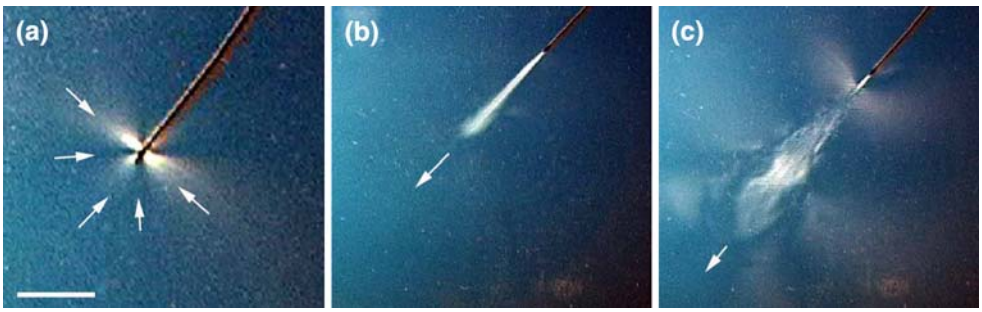

Fig. 8 A sink (**a**) and a source (**b, c**) generated by a 1-mm-diameter syringe inserted into a tank of dilute TMV solution. (**a**) The *white arrows* denote the direction of the flow. (**b**) At low speeds (15 cm/s), the jet remains laminar; (**c**), at high speeds (30 cm/s), the jet grows turbulent. *Scale bar* 1 cm

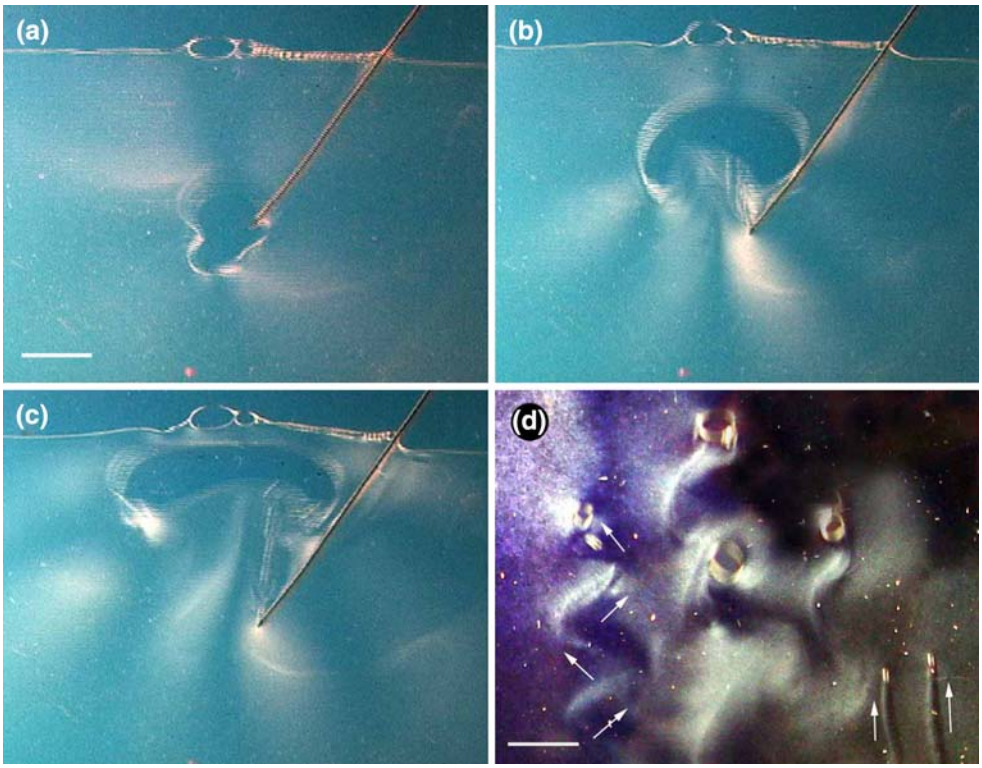

Fig. 9 Bubbles in a TMV solution bound in a thin gap. In (**a–c**), a large bubble is ejected from a syringe, approaching the form of a spherical cap before surfacing. Time between frames, 1/10 s. (**d**) The trajectory of rising bubbles is visualized by TMV and marked by the *arrows*. Large bubbles (3-mm diameter) follow a zig-zag path, leaving a Karman vortex street in their wake, while smaller bubbles rise vertically. *Scale bar* 1 cm

differential methods like DPIV, which characterizes the flow using positional differences between tracer particles. DPIV, while effective, has limitations. It is expensive computationally and its sensitivity is limited by the minimum motion that can be detected, which is a function of the illumination, brightness of the particle reflection and speed of the camera. We have shown that birefringent techniques like TMV, while qualitative, are attractive for several reasons.

First, organically derived TMV is safe for use with animals, making it appropriate for bio-fluid applications. Moreover, the fluid is transparent when viewed with the naked eye, allowing one to simultaneously record the motion of the creature and the flows it generates. Another advantage of TMV is its nanometer-size, making it attractive for microfluidic applications (Stone et al. 2004; Squires and Quake 2005). The TMV particles, 100 nm in length, are 10^2-10^3 times smaller than the average-sized tracer particle used in DPIV. Moreover, only a low concentration is needed (18 parts per million) to generate continuous flow field data.

TMV may find application in situations where DPIV provides insufficient resolution, specifically in areas of

extremely rapid, small scale, or spatially variable flow. We have shown that TMV can visualize flows on scales less than 1 mm, such as the rising of microbubbles or the suction flows into a fish's mouth. TMV methods might also complement work on the boundary layers around fish (Andersen 2001), flagellar swimming, the motion of dinoflagellates or food capture by copepod zooplankton (J. R. Strickler, pers. comm.). A recent paper used DPIV to visualize flow around models of swift wings in a flume at different Reynolds numbers and angles of attack, and revealed that lift, drag, and mobility were related to whether leading edge vortices were attached or separated (Videler et al. 2004). This system could be more directly imaged with TMV flow visualizations, as parameters are continuously altered to identify transition thresholds. Finally, high-speed cinematography could be used in conjunction with TMV to study the evolution and decay of short-lived vortices and their effects on propulsion, prey tracking, and prey capture.

TMV flow visualization techniques have the potential to provide a wealth of new imagery revealing subtle details of fluid flow patterns heretofore invisible or poorly visualized, which may shed valuable light on many biological problems including mechanisms of swimming, changes in modes of swimming, prey tracking, chemotaxis, prey capture, feeding in both motile and sessile marine organisms, and interactions between schooling organisms.

Acknowledgments We thank L. Mendel and B. Chan for assistance with experiments. TMV was kindly donated by S. Winter and M. Schönfelder of German Collection of Microorganisms and cell cultures (DSMZ). We thank Rudi Strickler and Gerald Stubbs for helpful conversations about the limitations of fluid visualization techniques and the physical properties of TMV respectively. T.G. gratefully acknowledges many conversations with the late F. W. Goro about the original photographs. We dedicate this paper to the memory of his pioneering work. J.W.M.B. gratefully acknowledges the financial support of the NSF.

References

Alcock ED, Sadron CL (1935) An optical method for measuring the distribution of velocity gradients in a two-dimensional flow. J Appl Phys 6:92–95

Andersen EJ, McGillis WR, Grosenbaugh MA (2001) The boundary layer of swimming fish. J Exp Biol 204:81–102

Bartol IK, Patterson MR, Mann R (2001) Swimming mechanics and behavior of the shallow-water brief squid *Lolliguncula brevis*. J Exp Biol 204:3655–3682

Bawden FC, Pirie NW, Bernal JD, Fankuchen I (1936) Liquid crystalline substances from virus-infected plants. Nature 138:1051

Boedtker H, Simmons NS (1958) The preparation and characterization of essentially uniform tobacco mosaic virus p. J Am Chem Soc 80:2550–2556

Binnie AM (1945) A double-refraction method of detecting turbulence in liquids. Proc Phys Soc 57:390–402

Cerf R, Scheraga HA (1952) Flow birefringence in solutions of macromolecules. Chem Rev 51:185–261

Dabiri JO, Colin SP, Costello JH, Gharib M (2005) Flow patterns generated by oblate medusan jellyfish: field measurements and laboratory analyses. J Exp Biol 208:1257–1265

Diesselhorst VH, Freundlich H (1916) Uber schlierenbildung in kolloiden losungen und ein verfahren die gestalt von kolloidteilschen festzustellen. Physik Zeitschr 17:117–128

Dorgan KM, Jumars PA, Johnson B, Boudreau BP, Landis E (2005) Burrow elongation by crack propagation. Nature 433:475

Drucker EG, Lauder GV (1999) Locomotor forces on a swimming fish: three-dimensional vortex wake dynamics quantified using digital particle image velocimetry. J Exp Biol 202:2393–2412

Fiedler H, Nottmeyere K (1985) Schlieren photography of water flow. Exp Fluids 3:145–151

Freundlich H (1926) Colloid and capillary chemistry. (trans: Hatfield HS). E.P. Dutton and Co., New York, pp 403–408

Goreau TJF, Goreau PDE, Goreau CSH (1993) On the nature of things: the scientific photography of Fritz Goro. Aperture Books, New York, pp 74–75

Full R, Yamauchi A, Jindrich D (1995) Maximum single leg force production: cockroaches righting on photoelastic gelatin. J Exp Biol 198:2441–2452

Hu DL, Chan B, Bush JWM (2003) The hydrodynamics of water strider locomotion. Nature 424:663–666

Humphrey RH (1922) Demonstration of the double refraction due to motion of a vanadium pentoxide sol, and some applications. Proc Phys Soc Lond 35:217–218

Maxwell JC (1873) On double refraction in a viscous fluid in motion. Proc Roy Soc (Lond) 22:46

McCutchen CW (1977) Froude propulsive efficiency of a small fish, measured by wake visualization. In: Pedley T (ed) Scale effects in animal locomotion. Academic Press, London, pp 339–363

Merzkirch W (1974) Flow Visualization. Academic Press, New York

Muller UK, Van den Heuvel BLE, Stamhuis EJ, Videler JJ (1997) Fish foot prints: morphology and energetics of the wake behind a continuously swimming mullet (*Chelon labrosus Risso*). J Exp Biol 200:2893–2906

Pindera JT, Krishnamurthy AR (1978) Characteristic relations of flow birefringence. Exp Mech 18:1–10

Prados JW, Peebles FN (1958) Two-dimensional laminar-flow analysis utilizing a birefringent liquid. AIChE J 5:225–234

Peterlin A (1976) Optical effects in flow. Annu Rev Fluid Mech 8:35–55

Pih H (1980) Birefringent-fluid-flow method in engineering. Exp Mech 20:437–444

Rosen M (1959) Water flow about a swimming fish. NOTS Technical Publication. U.S. Naval Ordnance Test Station, China Lake

Spedding GR, Hedenstrőm A, Rosén M (2003) Quantitative studies of the wakes of freely-flying birds in a low turbulence wind tunnel. Exp Fluids 34:291–303

Stamhuis EJ, Videler JJ (1995) Quantitative flow analysis around aquatic animals using laser sheet particle image velocimetry. J Exp Biol 198:283–294

Stone HA, Stroock AD, Ajdari A (2004) Engineering flows in small devices: microfluidics toward a lab-on-a-chip. Ann Rev Fluid Mech 36:381–411

Squires TM, Quake SR (2005) Microfluidics: fluid physics on the nanoliter scale. Rev Mod Phys 77:977–1026

Sutera SP (1960) Streaming birefringence as a hydrodynamic research tool. PhD. thesis, Cal Inst Tech

Takahashi WN, Rawlins TE (1933) Rod-shaped particles in tobacco mosaic virus demonstrated by stream double refraction. Science 77:26–27

Videler JJ, Stamhuis EJ, Povel GDE (2004) Leading-edge vortex lifts swifts. Science 306:1960–1962

Videler JJ, Muller UK, Stamhuis EJ (1999) Aquatic vertebrate locomotion: wakes from body waves. J Exp Biol 202:3423–3430
Wada E (1954) Effect of rate of shear on viscosity of a dilute linear polymer and of tobacco mosaic virus in solution. J Poly Sci 14:305–307
Wayland H (1960) Streaming birefringence of rigid macromolecules in geneal two-dimensional laminar flow. J Chem Phys 33:769–773
Welsh RE (1955) Studies on the aggregation reactions and basic dye binding of tobacco mosaic virus. J Gen Physiol 39:437–471
Zocher H (1921) Ueber Sole mit nichtkugeligen Teilchen [Sols with non-spherical particles]. Zeitschrift für physikalische Chemie 98:293–337